(Received 3 January 2024, Accepted 26 February 2024, Scheduled 14 March 2024)

Design of an Octave-Multimode Hybrid Broadband High-Efficiency Power Amplifier

Zuqiang Zhang*, Shiwei Zhao, Songlin Li, Longfei Zhou, Fei Zhao, and Jialin Li

Electromagnetic Field and Wireless Technology Innovation Laboratory
Chongqing University of Posts and Telecommunications
Chongqing, China

ABSTRACT: This paper discusses the challenges faced by existing power amplifier configurations in meeting the bandwidth requirements of modern communication technology while maintaining high efficiency due to the overlap of fundamental and harmonic frequencies. To address this issue, the paper proposes a matching method based on mode combination theory that utilizes the overlap of harmonic and fundamental impedance to simplify the design of broadband amplifiers. In this paper, a Chebyshev low-pass filter is used to control the higher harmonics instead of the conventional quarter-wavelength harmonic control network with a combination of harmonic impedances. The proposed method combines three modes of Resistive-Reactive class F [−1], class J, and class F power amplifiers, which can achieve high efficiency and octave frequency at the same time. The paper verifies the proposed method by designing and fabricating a multi-multiplier power amplifier with a drain efficiency of 61.8-73.9%, an operating bandwidth of 1.4–2.9 GHz, and a saturation output of 41.1–42.3 dBm. The amplifier also has a gain greater than 11.1–12.3 dBm, and at an output power of 36 dBm, the ACPR value is −32 to −33.1 dBc across the band.

1. INTRODUCTION

As wireless communication technology continues to advance, there is a growing need for communication systems with multi-band broadband capabilities. The ability to operate with high efficiency and across a wide range of frequencies is crucial for the front-end RF module of transceivers. As a result, the design of efficient broadband power amplifiers has become a key area of research in recent years.

In the cited references, trade-offs are observed between efficiency and bandwidth when combining power amplifier modes. However, most designs of output matching circuits are limited by bandwidth and exhibit low average efficiency across the frequency band due to the quarter-wavelength approach [10–12]. To address this, we have developed a multimode hybrid class bandwidth amplifier utilizing a filter principle. By incorporating a low-pass filter with a step impedance structure, our circuit effectively controls the multifrequency harmonic impedance, resulting in a highly efficient broadband output matching circuit.

One way to achieve high-efficiency broadband amplification is through the continuous class mode of the amplifier. However, as the demand for bandwidth increases, limitations arise, particularly when the bandwidth exceeds one octave. To address this, the mode combination theory has been developed, which involves combining multiple amplifier modes to increase design flexibility and achieve wideband, high-efficiency amplification.

* Corresponding author: Zuqiang Zhang (cyzhangzq@163.com).

2. THEORETICAL ANALYSIS

Traditional continuous-class power amplifiers [13] use a reactance factor to increase the voltage expression of a high-efficiency amplifier. Unfortunately, this approach only widens the fundamental matching region and extends the second harmonic impedance to the edge of the Smith circle diagram. It is challenging to achieve both fundamental impedance matching and second harmonic matching across a broad range of frequencies using pure reactance. Carruba et al. proposed to introduce the real part of the second harmonic by adding a resistance term $(1+\delta\cos(\theta))$ to the reactance factor [14]. This amplifier mode became the resistive reactance continuum class amplifier mode.

$$v_{DRRJ}(\theta) = V_{DD}(1-\cos\theta)(1-\gamma\sin\theta)(1+\delta\cos\theta) \quad -1\le\gamma\le1, 0\le\delta\le1 \tag{1}$$

$$i_{D,B}(\theta) = I_{\max}\left(\frac{1}{\pi}+\frac{1}{2}\cos\theta+\frac{2}{3\pi}\cos2\theta-\frac{2}{15\pi}\cos4\theta+\cdots\right) \tag{2}$$

Equation (1) expresses the voltage of a Resistive Reactance Class J Power Amplifier (RRJPA) [15], where the range of γ is from -1 to 1, and the range of δ is from 0 to 1.

Expression for drain current in standard class B power amplifier mode is designated as Equation (2).

The expression for the fundamental impedance and the expression for the second harmonic impedance of the RRJPA can be calculated from Equations (1) and (2). Equations (3) and (4) are the fundamental and harmonic wave impedance expressions for the RRJPA.

$$Z_{1,RRJ} = R_{opt}\left((1-\delta)+j\gamma\left(1-\frac{\delta}{4}\right)\right) \tag{3}$$

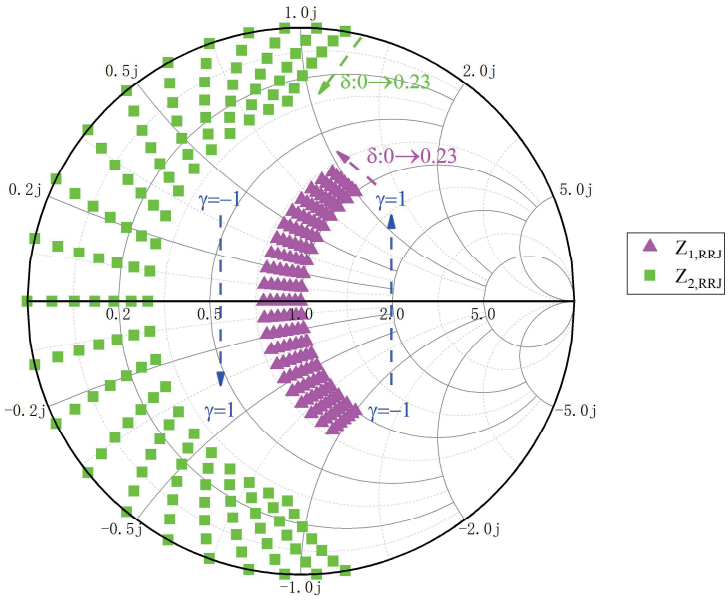

FIGURE 1. Impedance design space for RRJP.

$$Z_{2,RRJ} = \frac{3\pi}{8} R_{\text{opt}} \left(\delta - j\gamma\left(1-\delta\right)\right) \tag{4}$$

From Equations (1) and (2), its output power expression, tributary power expression, and efficiency expression can be calculated. Equations (5), (6), and (7) are the output power expression, DC power expression, and efficiency expression for the RRJPA, respectively.

Due to the introduction of impedance factor 1, the real part of the expression 1 kind of voltage is no longer 0 when $\delta \neq 0$, but is related to δ, so the obtained DC power consumption is lower than the actual situation. Since V_{DD} is a constant value in the real case and does not vary with δ, the actual DC power of the RRJPA should be corrected.

$$P_{1,RRJ} = \frac{(1-\delta)}{4} V_{DD} I_{\max} \tag{5}$$

$$P_{DC,RRJ} = \left(1-\frac{\delta}{2}\right)\frac{V_{DD} I_{\max}}{\pi} \tag{6}$$

$$\eta_{DE,RRJ} = \frac{\pi\left(1-\delta\right)}{4-2\delta} \cdot 100\% \tag{7}$$

Equation (8) is the modified DC power expression. From the modified DC power expression the modified efficiency expression can be directly introduced. Equation (9) is the modified efficiency expression.

$$P_{DC,RRJ} = \frac{V_{DD} I_{\max}}{\pi} \tag{8}$$

$$\eta_{RRJ} = \frac{\pi}{4}(1-\delta)\cdot 100\% \tag{9}$$

To make the drain efficiency of the amplifier in this mode greater than 60%, the value of δ is taken in the range of [0, 0.23]. The impedance design space of RRJPA can be drawn in terms of the range of values of δ. Fig. 1 shows the impedance design space of the RRJPA.

Equation (10) is the voltage expression for Resistive Reactance Class F Power Amplifier (RRFPA) [16]. Similarly, the fundamental impedance expression and harmonic impedance expression of the RRFPA can be derived from Equations (2) and (10). Equations (11)–(13) are the fundamental wave impedance expression and harmonic wave impedance expression of RRFPA.

$$v_{DRRF}(\theta) = V_{DD}(1-\alpha\cos\theta+\beta\cos 3\theta)(1-\gamma\sin\theta)(1+\delta\cos\theta) \tag{10}$$

$$Z_{1,RRF} = R_{opt}\left(\left(\frac{2}{\sqrt{3}}-\delta\right)+j\gamma\left(1-\frac{\left(\frac{2}{\sqrt{3}}+\frac{1}{3\sqrt{3}}\right)\delta}{4}\right)\right) \tag{11}$$

$$Z_{2,RRF} = \frac{3\pi}{8} R_{opt}\left(\left(\frac{2}{\sqrt{3}}-\frac{1}{3\sqrt{3}}\right)\delta - j\gamma\left(\frac{2}{\sqrt{3}}+\frac{1}{3\sqrt{3}}-\delta\right)\right) \tag{12}$$

$$Z_{3,RRF} = \infty \tag{13}$$

$$\eta_{RRF} = \frac{2-\sqrt{3}\delta}{4\sqrt{3}}\pi\cdot 100\% \tag{14}$$

As with RRJPA, the efficiency expression for RRFPA needs to be corrected. Equation (14) is the efficiency expression for the corrected RRFPA.

To make the efficiency of the amplifier in the mode of RRFPA higher than 60%, the value of δ is in the range of [0, 0.39]. The impedance design space of RRFPA can be drawn in terms of the range of values of δ. Fig. 2 shows the impedance design space of the RRFPA.

As with the derivation of RRJPA, the conductance expression for RRIFPA and its corresponding impedance design space are given below. The range of δ in the conductivity expression is [0, 0.4].

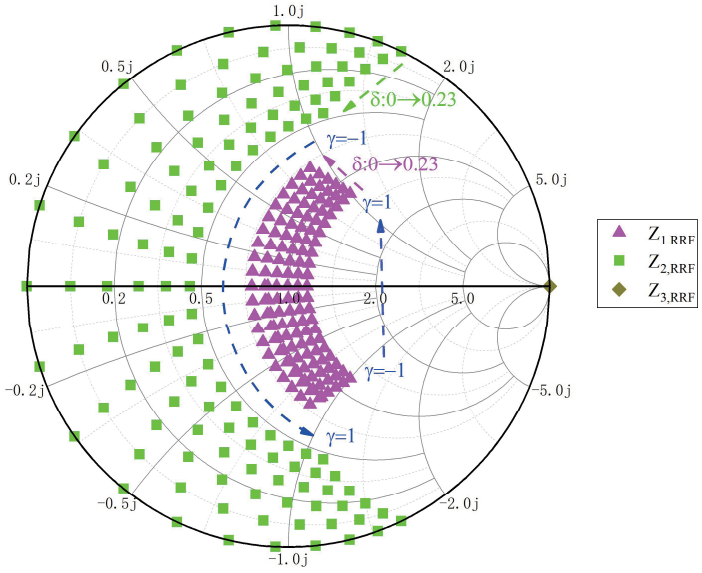

FIGURE 2. Impedance design space for RRFPA.

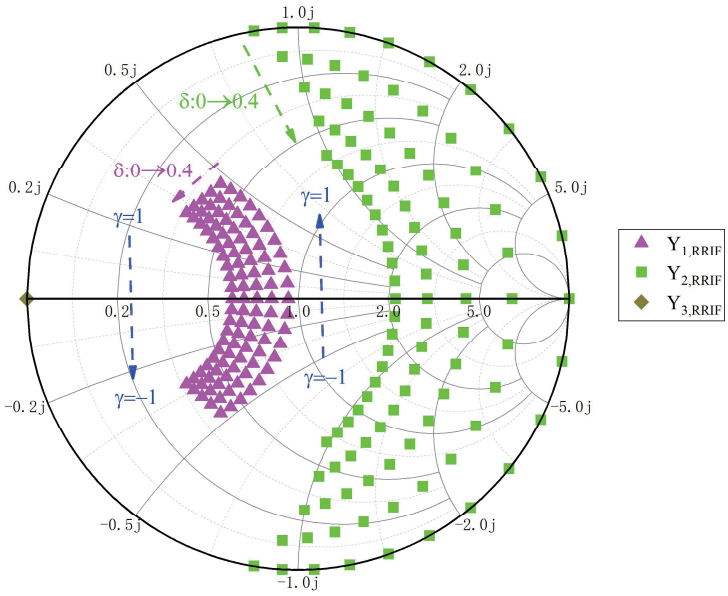

FIGURE 3. Impedance design space for RRIFPA.

Equations (15)–(17) are the conductance expressions for Resistive Reactance Inverse Class F Power Amplifier (RRIFPA) [17], and Fig. 3 shows the impedance design space.

$$Y_{1,} = \sqrt{2}\left(\left(1.16-\delta\right)-j\left(0.33\delta\gamma-\gamma\right)\right)G_{opt} \quad (15)$$

$$Y_{2,f\_u} = 2\left(\delta-j\left(1.32-\delta\right)\gamma\right)G_{opt} \quad (16)$$

$$Y_{3,f\_u} = \infty \quad (17)$$

Based on the principles of microwave transmission circuits and related knowledge, we can observe that the phase of microwave transmission circuits typically exhibits a clockwise rotation trend with increasing frequency. This characteristic closely resembles the frequency response characteristics of capacitive inductors. It is worth noting that the analysis of microwave transmission principles often utilizes an equivalent LC circuit model.

3. MATCHING NETWORK CIRCUIT DESIGN

Based on the theoretical analysis presented above, it is evident that the different modes of the power amplifier require harmonic conditions that overlap. This overlapping enables the combination of modes from multiple power amplifiers. Additionally, the low-pass filter exhibits an all-reflective characteristic outside of the passband, which demonstrates reactance properties in transmission line theory [18–21]. As a result, the

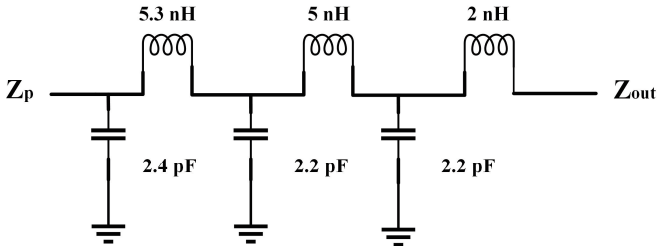

FIGURE 4. Lumped parameter circuit.

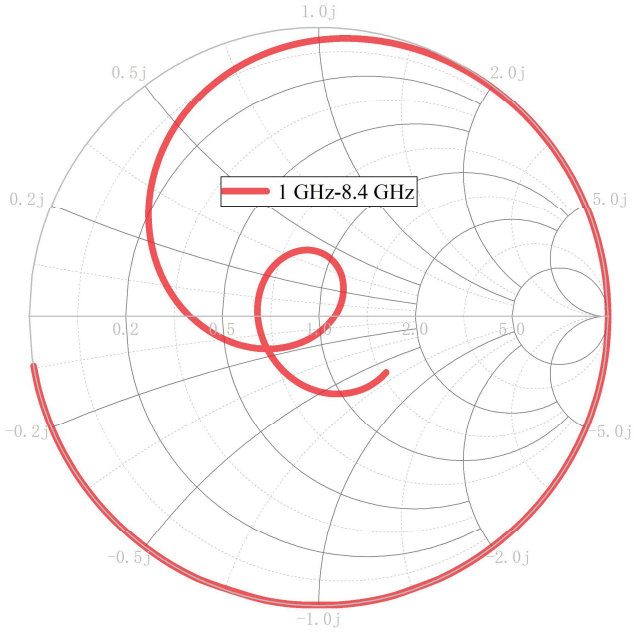

FIGURE 5. Impedance trace of amplifier drain tip.

higher harmonics are located on the periphery of the Smith circle diagram. By utilizing a low-pass filter instead of the conventional $\lambda/4$ line to manage the higher harmonics, the amplifier design becomes less complex.

By leveraging the unique features of the CG2H40010F transistor and taking into account the desired bandwidth outlined in this paper, a six-stage low-pass filter was chosen for implementation [22–27]. This sixth-order filter effectively exhibits favorable passband properties and can effectively reject high-frequencies within the 1.7 GHz range. Refer to Fig. 4 for a visual depiction of the selected parameters, which were based on both passband bandwidth and high-frequency rejection characteristics.

To ensure optimal performance of a distributed element impedance matching circuit, it is recommended that the collector element is initially converted to a distributed element. This can be achieved by applying the transformation equations outlined in [14], which convert aggregate parameter circuits into distributed parameter circuits. Once being transformed, the impedance traces at the drain extremity of the power amplifier can be simulated, with results displayed in Fig. 5.

By examining Fig. 5, it is evident that both fundamental matching and harmonic suppression are improved. Due to the presence of discontinuities in circuits, the designer must make appropriate adjustments to the physical components of the circuit. In this case, a step impedance structure is employed to achieve the matching circuit. The cascade structure is uncomplicated and trustworthy, making it favorable for the amplifier's subsequent debugging.

4. IMPLEMENTATION AND MEASUREMENT

To assess the feasibility of the resistive hybrid continuum class amplifier proposed in this paper, simulations are conducted using Advanced Design System (ADS), and measurements are made through machining. A power amplifier operating at 1.2–2.9 GHz was designed and fabricated using Rogers 4350B ($H = 0.762$ mm, $r = 3.66$) and RFJFET transistor CG2H40010F. The gate bias voltage is -2.7 V, and the drain bias voltage is 28 V. Fig. 6 shows the dimensional drawing of the power amplifier designed in this paper, and Fig. 7 shows the physical drawing. The capacitor C in Fig. 6 is 4.7 pF, and the resistor R is 50 ohms.

The amplifier is operated using continuous wave signal excitation in the range of 1.4 to 2.9 GHz, and the simulation and measurement results are shown in Fig. 8.

It can be observed that the measured DE is 61.8–73.9%; the measured output power is 41.1–42.3 dBm; and the mea-

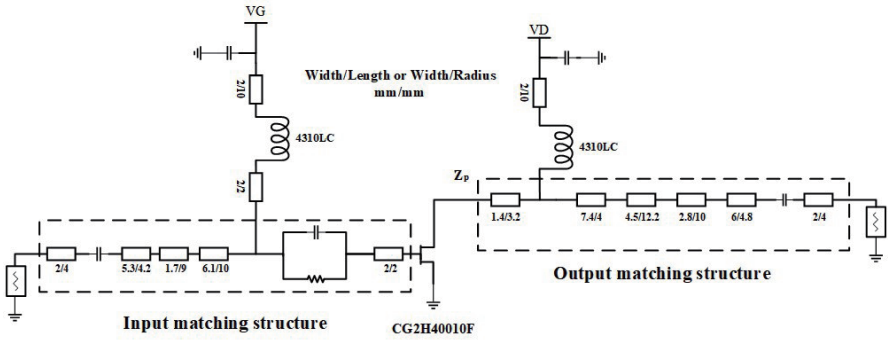

FIGURE 6. Overall circuit dimensions of the power amplifier.

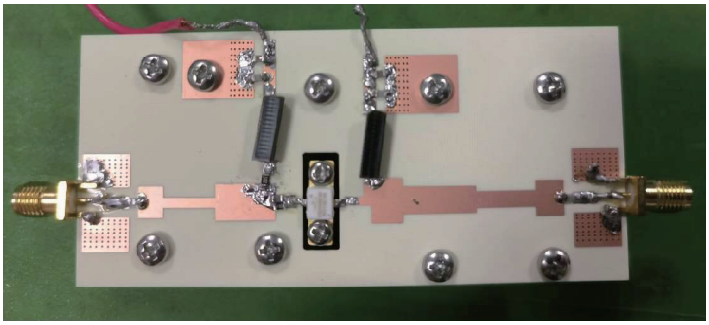

FIGURE 7. Physical drawing of the power amplifier.

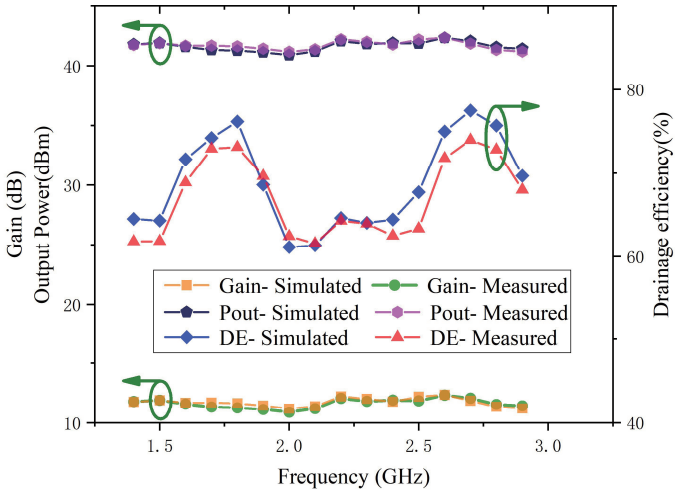

FIGURE 8. Simulation and test result graph.

sured gain is 11.1–12.3 dB over the entire 1.4 GHz–2.9 GHz band. Since the second harmonic impedance around 1.8 GHz in the band is closer to the short-circuit point and the third harmonic impedance closer to the open-circuit point, the lower the δ is, the higher the DE is. Since the second harmonic around 2.7 GHz is closer to the open-circuit point and the third harmonic closer to the short-circuit point, the lower the δ is, the higher the DE is.

The current-voltage waveforms for 1.8 GHz, 2.2 GHz, and 2.7 GHz are given below. Fig. 9(a) shows the voltage-current waveforms at the drain of the power amplifier operating at 1.8 GHz. From the figure, it can be seen that the current waveform approximates a sinusoidal waveform; the voltage approximates a square waveform; and the amplifier operates in resistive reactance continuous class F mode. Fig. 9(b) shows the voltage-current waveforms at the drain of the power amplifier operating at 2.2 GHz. From the figure, it can be seen that the current waveform approximates a sinusoidal waveform; the voltage approximates a sinusoidal waveform; and the power amplifier operates in resistive reactance class J mode. Fig. 9(c) shows the voltage-current waveforms at the drain of the power amplifier operating at 2.7 GHz. From the figure, it can be seen that the current waveform approximates a square wave; the voltage ap-

TABLE 1. Comparison with other referenced power amplifiers.

References	Bandwidth (GHz)/Percentage bandwidth	Efficiency	Output power (dBm)	Gain (dB)
[1]	3.5–5.5 GHz / 44%	56–70%	39.7–41.2	8.6–10.2
[3]	2.4–4 GHz / 50%	55.6–75.4%	39.6–41.4	10.7–12.5
[7]	2.5–3.5 GHz/ 33%	68%	39.84	9.84
[8]	1.65–2.75 GHz/ 50%	46-62%	44.5–46.3	-
[9]	1.7–2.3 GHz/ 30%	50%	36	15
This work	1.4–2.9 GHz/ 70%	61.8–73.9%	41.1–42.3	11.1–12.3

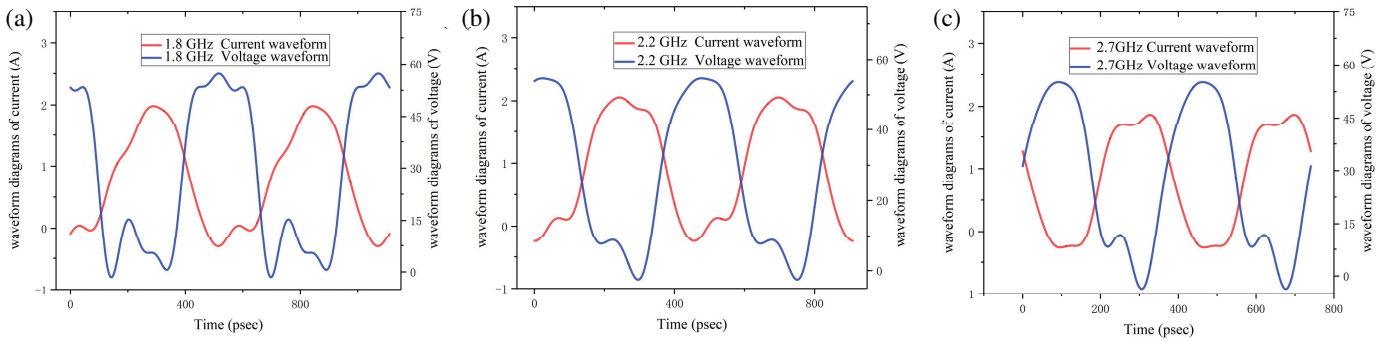

FIGURE 9. Voltage and current waveforms.

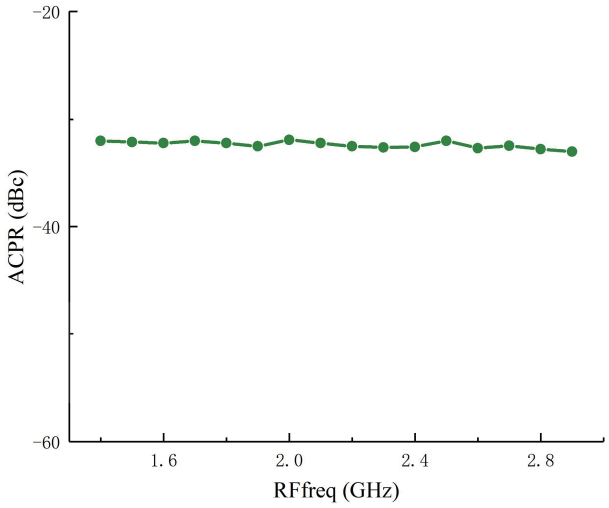

FIGURE 10. ACPR value at an output power of 36 dBm.

proximates a sinusoidal wave; and the amplifier operates in resistive inverse class F mode.

Figure 10 shows the adjacent channel power ratio (ACPR) in the operating band of the power amplifier. The linearity of the power amplifier was tested using a 20 MHz LTE signal with a peak average power of 7.6 dB. The results show that at an output power of 36 dBm, the ACPR value is −32 to −33.1 dBc across the band. The linearity of the amplifier can be improved by digital pre-distortion technology [28].

Table 1 lists the comparisons of some published broadband power amplifiers with the present work, and it can be seen that the performance of the hybrid continuous class power amplifier designed in this paper is superior to other power amplifiers. Considering the output power, efficiency, bandwidth, and other indicators, it can be seen that the proposed hybrid continuous-class power amplifier is more suitable for practical applications.

5. CONCLUSION

This paper presents the design of a multimode hybrid high-efficiency broadband power amplifier for amplification. The high-frequency rejection characteristics of the low-pass filter are utilized instead of the traditional $\lambda/4$ to adjust the harmonic impedance, and the harmonic impedance is adjusted while the fundamental matching is realized, and multiple high-efficiency

amplifier modes are combined to improve the bandwidth and efficiency. Finally, a power amplifier operating at 1.4–2.9 GHz is designed and fabricated. The measured results show that the drain efficiency is 61.8–73.9%; the output power is 41.1–42.3 dBm; the gain is 11.1–12.3 dB; and the relative bandwidth is 70%. The design method is a practical reference for the design of broadband high-efficiency power amplifiers.

ACKNOWLEDGEMENT

Supported by Science and Technology Innovation Key R&D Program of Chongqing (CSTB2023TIAD-STX00I7).

REFERENCES

[1] Feng, W., W. Wu, X. Y. Zhou, W. Che, and Y. Shi, "Broadband high-efficiency quasi-class-J power amplifier based on nonlinear output capacitance effect," *IEEE Transactions on Circuits and Systems II: Express Briefs*, Vol. 69, No. 4, 2091–2095, Apr. 2022.

[2] Sharma, T., R. Darraji, F. Ghannouchi, and N. Dawar, "Generalized continuous class-F harmonic tuned power amplifiers," *IEEE Microwave and Wireless Components Letters*, Vol. 26, No. 3, 213–215, Mar. 2016.

[3] Shi, W., S. He, and Q. Li, "A series of inverse continuous modes for designing broadband power amplifiers," *IEEE Microwave and Wireless Components Letters*, Vol. 26, No. 7, 525–527, Jul. 2016.

[4] Dong, Y., L. Mao, and S. Xie, "Extended continuous inverse class-F power amplifiers with class-AB bias conditions," *IEEE Microwave and Wireless Components Letters*, Vol. 27, No. 4, 368–370, Apr. 2017.

[5] Yang, Z., Y. Yao, M. Li, Y. Jin, T. Li, Z. Geng, and Z. Yu, "A precise harmonic control technique for high efficiency concurrent dual-band continuous Class-F power amplifier," *IEEE Access*, Vol. 6, 51 864–51 874, 2018.

[6] Wright, P., J. Lees, J. Benedikt, P. J. Tasker, and S. C. Cripps, "A methodology for realizing high efficiency class-J in a linear and broadband PA," *IEEE Transactions on Microwave Theory and Techniques*, Vol. 57, No. 12, 3196–3204, Dec. 2009.

[7] Tubitak, E. C., O. Palamutcuogullan, O. K. Tubitak, B. S. Yarman, and M. Yazgi, "High efficiency wideband power amplifier with class-J configuration," in *2018 18th Mediterranean Microwave Symposium (MMS)*, 394–397, Istanbul, Turkey, 2018.

[8] Chen, X., W. Chen, F. M. Ghannouchi, Z. Feng, and Y. Liu, "A broadband doherty power amplifier based on continuous-mode technology," *IEEE Transactions on Microwave Theory and Techniques*, Vol. 64, No. 12, 4505–4517, Dec. 2016.

[9] Amirpour, R., R. Darraji, F. Ghannouchi, and R. Quay, "Enhancement of the broadband efficiency of a class-J power amplifier with varactor-based dynamic load modulation," *IEEE Microwave and Wireless Components Letters*, Vol. 27, No. 2, 180–182, Feb. 2017.

[10] Liu, G., C. Guo, Z. Cheng, Z. Zhang, G. Zhou, and W. Zhao, "A broadband class-F/J hybrid power amplifier," *Microwave and Optical Technology Letters*, Vol. 62, No. 7, 2518–2524, Jul. 2020.

[11] Moon, J., S. Jee, J. Kim, J. Kim, and B. Kim, "Behaviors of class-F and class-F-1 amplifiers," *IEEE Transactions on Microwave Theory and Techniques*, Vol. 60, No. 6, 1937–1951, Jun. 2012.

[12] Tong, R., S. He, B. Zhang, Z. Jiang, X. Hou, and F. You, "A novel topology of matching network for realizing broadband high efficiency continuous class-f power amplifiers," in *2013 European Microwave Integrated Circuit Conference*, 1475–1478, Nuremberg, Germany, Oct. 2013.

[13] Kim, K. and H. Choi, "High-efficiency high-voltage class F amplifier for high-frequency wireless ultrasound systems," *PLoS One*, Vol. 16, No. 3, e0249034, Mar. 2021.

[14] Carrubba, V., M. Akmal, R. Quay, J. Lees, J. Benedikt, S. C. Cripps, and P. J. Tasker, "The continuous inverse class-F mode with resistive second-harmonic impedance," *IEEE Transactions on Microwave Theory and Techniques*, Vol. 60, No. 6, 1928–1936, Jun. 2012.

[15] Friesicke, C., R. Quay, and A. F. Jacob, "The resistive-reactive class-J power amplifier mode," *IEEE Microwave and Wireless Components Letters*, Vol. 25, No. 10, 666–668, Oct. 2015.

[16] Zheng, S. Y., Z. W. Liu, X. Y. Zhang, X. Y. Zhou, and W. S. Chan, "Design of ultrawideband high-efficiency extended continuous class-F power amplifier," *IEEE Transactions on Industrial Electronics*, Vol. 65, No. 6, 4661–4669, Jun. 2018.

[17] Tang, Q.-H., Y.-H. Li, and W.-G. Li, "Over second octave power amplifier design based on resistive–resistive series of continuous class-F/F−1 modes," *IEEE Microwave and Wireless Components Letters*, Vol. 27, No. 5, 494–496, May 2017.

[18] Chen, K. and D. Peroulis, "Design of highly efficient broadband class-E power amplifier using synthesized low-pass matching networks," *IEEE Transactions on Microwave Theory and Techniques*, Vol. 59, No. 12, 3162–3173, Dec. 2011.

[19] Chen, K. and D. Peroulis, "Design of broadband highly efficient harmonic-tuned power amplifier using in-band continuous class-F-1/F mode transferring," *IEEE Transactions on Microwave Theory and Techniques*, Vol. 60, No. 12, 4107–4116, Dec. 2012.

[20] Matthaei, G. L., "Tables of chebyshev impedance-transforming networks of low-pass filter form," *Proceedings of the IEEE*, Vol. 52, No. 8, 939–963, 1964.

[21] Cristal, E. G., "Tables of maximally flat impedance-transforming networks of low-pass-filter form (correspondence)," *IEEE Transactions on Microwave Theory and Techniques*, Vol. 13, No. 5, 693–695, 1965.

[22] Fano, R. M., "Theoretical limitations on the broadband matching of arbitrary impedances," *Journal of the Franklin Institute*, Vol. 249, No. 1, 57–83, 1950.

[23] Dawson, D. E., "Closed-form solutions for the design of optimum matching networks," *IEEE Transactions on Microwave Theory and Techniques*, Vol. 57, No. 1, 121–129, Jan. 2009.

[24] Levy, R., "Explicit formulas for chebyshev impedance-matching networks, filters and interstages," in *Proceedings of the Institution of Electrical Engineers*, Vol. 111, No. 6, 1099–1106, 1964.

[25] Matthaei, G., "Synthesis of Tchebycheff impedance-matching networks, filters, and interstages," *IRE Transactions on Circuit Theory*, Vol. 3, No. 3, 163–172, 1956.

[26] Matthaei, G. L., "Design of wide-band (and narrow-band) band-pass microwave filters on the insertion loss basis," *IRE Transactions on Microwave Theory and Techniques*, Vol. 8, No. 6, 580–593, 1960.

[27] Wright, P., J. Lees, J. Benedikt, P. J. Tasker, and S. C. Cripps, "A methodology for realizing high efficiency class-J in a linear and broadband PA," *IEEE Transactions on Microwave Theory and Techniques*, Vol. 57, No. 12, 3196–3204, Dec. 2009.

[28] Cao, H., H. M. Nemati, A. S. Tehrani, T. Eriksson, J. Grahn, and C. Fager, "Linearization of efficiency-optimized dynamic load modulation transmitter architectures," *IEEE Transactions on Microwave Theory and Techniques*, Vol. 58, No. 4, 873–881, Apr. 2010.